Journal of Physics:
Complexity

Criticality and network structure drive emergent oscillations in a stochastic whole-brain model

Journal of Physics: Complexity

OPEN ACCESS

PAPER

Criticality and network structure drive emergent oscillations in a stochastic whole-brain model

Giacomo Barzon[1,2,*,4], Giorgio Nicoletti[1,4], Benedetta Mariani[1,2], Marco Formentin[2,3] and Samir Suweis[1,2,*]

[1] Laboratory of Interdisciplinary Physics, Department of Physics and Astronomy 'G Galilei', University of Padova, Padova, Italy
[2] Padova Neuroscience Center, University of Padova, Padova, Italy
[3] Department of Mathematics 'Tullio Levi-Civita', University of Padova, Padova, Italy
[*] Authors to whom any correspondence should be addressed.
[4] These authors contributed equally to this work.

E-mail: giacomo.barzon.1@phd.unipd.it and samir.suweis@unipd.it

Keywords: brain criticality, brain networks, stochastic model, mean field, neural oscillations

RECEIVED
21 January 2022

REVISED
10 June 2022

ACCEPTED FOR PUBLICATION
20 June 2022

PUBLISHED
5 July 2022

Abstract

Understanding the relation between the structure of brain networks and their functions is a fundamental open question. Simple models of neural activity based on real anatomical networks have proven to be effective in describing features of whole-brain spontaneous activity when tuned at their critical point. In this work, we show that structural networks are indeed a crucial ingredient in the emergence of collective oscillations in a whole-brain stochastic model at criticality. We study analytically a stochastic Greenberg–Hastings cellular automaton in the mean-field limit, showing that it undergoes an abrupt phase transition with a bistable region. In particular, no global oscillations emerge in this limit. Then, we show that by introducing a network structure in the homeostatic normalization regime, the bistability may be disrupted, and the transition may become smooth. Concomitantly, through an interplay between network topology and weights, a large peak in the power spectrum appears around the transition point, signaling the emergence of collective oscillations. Hence, both the structure of brain networks and criticality are fundamental in driving the collective responses of whole-brain stochastic models.

1. Introduction

The human brain is an impressively complex system, spanning several spatial scales of organizations, from microcircuits to whole-brain networks. The comprehensive map of neural connections is usually referred to as 'connectome' [1]. However, it is typically unfeasible to reconstruct connectomes at the neuronal level, and often one relies on anatomical connectivity at coarser spatial scales. In humans, such brain structural networks are typically assessed with diffusion tensor/spectrum imaging techniques, which quantify white matter pathways between mesoscopic brain regions [2, 3].

These complex interconnections act as a backbone on top of which the neurophysiological dynamics occurs. One way to measure such neural activity is through functional magnetic resonance imaging (fMRI). Correlations in fMRI signals of spontaneous activity during rest have been repeatedly observed [4], yielding detailed maps of complex emergent patterns of coherent brain activities, called resting state (functional) networks [5]. Such patterns, consistent among healthy individuals [6], are specifically associated with neuronal systems responsible for sensory, cognitive, and behavioral functions [7, 8].

A hypothesis that is increasingly being considered in light of the growing experimental [9, 10] and theoretical [11, 12] results is that collective emergent patterns are signatures of brain self-organization at a *critical* point [13, 14], that is, the brain dynamics may be poised at the edge of a phase transition. Over the years, evidence to support this hypothesis emerged in the presence of scale-free neural avalanches [15] and cluster size distributions [16, 17], long-range temporal and spatial correlations [18, 19] during spontaneous brain activity—exemplary properties of a system near its critical point. Furthermore, it was recently shown that

the collective dynamics of neurons may be associated with a non-trivial fixed point of phenomenological renormalization groups [20, 21]. Some works have also suggested that this phenomenology is compatible with systems between an asynchronous and a synchronous phase, with emerging oscillations [22–24]. In all these studies the role of the network structure in driving such emerging patterns—e.g., global oscillations or optimal information processing—is often missing.

In fact, the emerging collective dynamics in the brain is shaped both by the underlying connectome and by neural population activities [25–27]. Despite a direct relation between structural and functional networks, to what extent structure does determine the neural dynamics and its critical signatures has still to be clarified [28, 29]. Computational models may be the key to bridging this gap [30]. To this end, biophysically inspired models of neural dynamics are typically built on top of empirically derived structural networks, with the aim of reconciling functional behavior.

Notably, a stochastic version of the Greenberg & Hastings (GH) cellular automaton [31]—one of the simplest models to describe neural dynamics—running over a human connectome of $N = 998$ cortical regions [32] was shown to match some features of whole-brain activity when tuned to the critical point [16, 18]. In fact, the model undergoes a critical percolation-like transition in the sizes of active clusters, as a function of the level of induced excitatory activation by neighboring neurons. Yet, it is known that geometrical percolation transitions may arise in stochastic dynamical systems, and they usually do not coincide with actual dynamical transitions [33]. In fact, a dynamical transition that separates a regime of low activity from an overactive phase is present beyond the static percolation transition, and less is known about it. Recent numerical studies have suggested that it may be continuous for certain levels of connectivity, otherwise being discontinuous or even absent [34]. Nevertheless, the mechanisms underlying this transition and a corresponding analytical description are still lacking. Here, we will focus on the presence and properties of this dynamical transition to better elucidate the relation between the network structure, brain criticality, and emergent collective oscillations.

To this aim, we develop a stochastic continuous-time formulation of the GH model via a master equation approach. We show analytically how two stable equilibria emerge in the mean-field limit, together with a bistable region of the parameter space where these two equilibria coexist. Hence, the mean-field limit predicts a discontinuous transition—i.e., a transition in which the order parameter displays a finite jump. Then, we derive the power spectrum of the oscillations and show that, in general, in the mean-field limit, no characteristic peak is present. That is, we do not observe neural activity with collective oscillations. However, when we go beyond the mean-field by adding a network connecting different brain regions, the picture is quite different. We find that the transition becomes continuous—i.e., the order parameter changes smoothly—and collective sustained oscillations emerge.

Overall, our results shed light on the role of the underlying network structure in the emergent collective patterns observed in the brain, as well as explain the mechanisms behind the phase diagram of the GH model reported in previous works [16, 18, 34–37].

2. Methods

2.1. Whole-brain stochastic continuous-time model

Here, we develop a continuous-time formulation of the whole brain stochastic model introduced by Haimovici *et al* [18] to describe the dynamics of the human brain at a mesoscopic scale. Such a model is a variation of the GH cellular automaton [31], originally designed to study excitable media. Briefly, each node in the system belongs to one of three states: quiescent Q, excited E, or refractory R. The original dynamics of the GH automaton is modified in such a way that the states undergo the following stochastic transitions:

$$\begin{cases} Q \to E & \text{if } \sum_j W_{ij} s_j(t) > T \text{ or with prob. } r_1 \\ E \to R & \text{with prob. } 1 \\ R \to Q & \text{with prob. } r_2, \end{cases} \tag{1}$$

where $s_j(t) \in \{0, 1\}$ is the state of node j at a certain time step t—set to 1 if the node is in the E state, and 0 otherwise—, W_{ij} is the weighted connectivity matrix of the underlying network, r_1 is the probability of self-activation and r_2 is the probability of recovery from the refractory state. In particular, T is a threshold that governs the induced activation due to interaction with neighboring nodes, which acts as a control parameter of the model.

Therefore, in this model, a neuron may be activated either if the weighted combined activity of neighboring neurons exceeds a threshold T, or it may self-activate with a probability r_1 that encodes, e.g., external stimuli or unobserved pathways. After activation, neurons switch to a refractory state with unitary probability and

cannot activate again. Finally, escape from the refractory state occurs with probability r_2. In this formulation, the state of the system evolves in discrete time steps and is updated synchronously. In particular, for small values of T, the activity spreads easily between neighboring nodes, even along weak connections. This leads to a regime of high and sustained activation, characterized by fast and temporally uncorrelated fluctuations. We refer to this phase as 'super-critical'. For high values of T, the activity is instead sustained only by few strong connections, resulting in a suppressed or 'sub-critical' phase with regular, short-propagating activity in which nodes fail to give rise to relevant patterns of activity. Importantly, we include homeostatic plasticity in the model, implemented as a normalization of the excitatory input of the incoming node. It has been shown that its addition improves the correspondence between simulated neural patterns and experimental brain functional data [16].

We now study analytically its continuous time mean-field behavior in the large N limit, together with its power spectrum in the stochastic linearized regime. Given a network of N units, we denote by $\sigma_i(t) \in \{E, R, Q\}$, $i = 1, \ldots, N$, the state of the site i at time t. The dynamics in (1) can be translated into the following continuous-time evolution: for $h > 0$ and each node i, the probability of having $\sigma_i(t+h) = E$ given that $\sigma_i(t) = Q$ is $r_{\text{act}}(i)h + o(h)$ where $r_{\text{act}}(i)$ is the rate of activation, defined as

$$r_{\text{act}}(i) = r_1 + (1 - r_1)\Theta\left[\sum_j W_{ij}s_j - T\right] \tag{2}$$

with $\Theta[\cdot]$ the Heaviside step function. Notice that $0 \leqslant r_1 \leqslant 1$ by construction. In a similar manner the probability of jumping from state E at time t to state R at time $t+h$ will be $h + o(h)$ and from R to Q will be $r_2 h + o(h)$.[5]

The mean-field approximation of the model corresponds to the assumption that the underlying graph is fully-connected with constant weights, i.e., $W_{ij} = c, \forall\, i, j$. In fact, considering the homeostatic normalization [16], the weights of the structural matrix are simply $\widetilde{W}_{ij} = W_{ij}/\sum_j W_{ij} = 1/N$. Thus the activation of a node due to the neighboring nodes is simply given by the density of active nodes in the network, i.e., the argument inside $\Theta[\cdot]$ in (2) becomes

$$\sum_j \widetilde{W}_{ij}s_j - T = \frac{n_{\text{E}}}{N} - T \tag{3}$$

and it is independent of the particular node i, i.e., $r_{\text{act}}(i) = r_{\text{act}}$.

These transition rules induce a Markovian dynamics on $n_{\text{E}}, n_{\text{R}}, n_{\text{Q}} = N - n_{\text{E}} - n_{\text{Q}}$—respectively the number of active, refractory, and inactive nodes—with the following rates:

$$\begin{aligned}
(n_{\text{E}}, n_{\text{R}}, n_{\text{Q}}) &\xrightarrow{n_{\text{Q}} r_{\text{act}}} (n_{\text{E}} + 1, n_{\text{R}}, n_{\text{Q}} - 1) \\
(n_{\text{E}}, n_{\text{R}}, n_{\text{Q}}) &\xrightarrow{n_{\text{E}}} (n_{\text{E}} - 1, n_{\text{R}} + 1, n_{\text{Q}}) \quad . \\
(n_{\text{E}}, n_{\text{R}}, n_{\text{Q}}) &\xrightarrow{n_{\text{R}} r_2} (n_{\text{E}}, n_{\text{R}} - 1, n_{\text{Q}} + 1)
\end{aligned} \tag{4}$$

Then, from the reactions in (4), we can write the master equation of our continuous-time model

$$\begin{aligned}
\dot{P}(n_{\text{E}}, n_{\text{R}}) = {} & P(n_{\text{E}} - 1, n_{\text{R}})[N - n_{\text{E}} - n_{\text{R}} + 1]r_{\text{act}} \\
& + P(n_{\text{E}} + 1, n_{\text{R}} - 1)[n_{\text{E}} + 1] \\
& + P(n_{\text{E}}, n_{\text{R}} + 1)[n_{\text{R}} + 1]r_2 \\
& - P(n_{\text{E}}, n_{\text{R}})[(N - n_{\text{E}} - n_{\text{R}})r_{\text{act}} + n_{\text{E}} + n_{\text{R}} r_2],
\end{aligned} \tag{5}$$

where $P(n_{\text{E}}, n_{\text{R}})$ is the joint probability of finding n_{E} active nodes and n_{R} refractory nodes.

2.2. Equilibria and power spectrum

In order to study analytically the dynamics given by the master equation (5), we perform its Kramers–Moyal expansion truncated at second order. In this way, we can derive the associated Fokker–Planck and Langevin equations [38]. The latter describes the stochastic evolution of the density of active $x = n_{\text{E}}/N$ and refractory $y = n_{\text{R}}/N$ nodes, which obeys

$$\begin{bmatrix} \dot{x} \\ \dot{y} \end{bmatrix} = \begin{bmatrix} A_1(x,y) \\ A_2(x,y) \end{bmatrix} + \frac{1}{\sqrt{N}} \begin{bmatrix} B_{11}(x,y)\, B_{12}(x,y) \\ B_{21}(x,y)\, B_{22}(x,y) \end{bmatrix}^{1/2} \begin{bmatrix} \xi_1 \\ \xi_2 \end{bmatrix}, \tag{6}$$

[5] We highlight that the parameters r_1 and r_2 in the time discrete model were probabilities, whereas here they are rates.

where $\boldsymbol{\xi} = [\xi_1, \xi_2]$ is an uncorrelated 2d white Gaussian noise, i.e., such that $\xi_i \sim N(0,1)$ and $\langle \xi_i(t)\xi_j(t')\rangle = \delta_{ij}\delta(t-t')$, $\boldsymbol{A}(x,y)$ is the deterministic drift term, and $\boldsymbol{B}(x,y)$ encloses the stochastic diffusive part (see appendix A for the full derivation).

To analytically investigate the oscillatory dynamics of our model, from (6) we perform a linear noise approximation [38] by defining the local coordinates (ζ_1, ζ_2) as

$$\begin{cases} x(t) = x^* + \dfrac{\zeta_x(t)}{\sqrt{N}} \\ y(t) = y^* + \dfrac{\zeta_y(t)}{\sqrt{N}} \end{cases} \Rightarrow \begin{cases} \zeta_x(t) = \sqrt{N}(x(t) - x^*) \\ \zeta_y(t) = \sqrt{N}(y(t) - y^*) \end{cases}. \tag{7}$$

Then (see appendix C for details) the power spectrum of the oscillations around a given equilibrium is given by

$$S_i(\omega) = \langle \tilde{\zeta}_i(\omega)\tilde{\zeta}_i^*(\omega)\rangle = \langle \tilde{\zeta}_i(\omega)\tilde{\zeta}_i(-\omega)\rangle \tag{8}$$

for $i = x, y$.

To test the validity of our analytical predictions, we simulate the dynamics of the continuous model with a discretization step of $\Delta t = 0.01$ starting from a random configuration of active and refractory neurons. The parameters $r_1 = 0.001$ and $r_2 = 0.1$ remain fixed in all simulations and are chosen to be similar to those used in previous works [16, 18, 34–37].

3. Results

3.1. Existence of a bistable region

In the limit of a large number of interacting units in the system, the effect of random fluctuations becomes negligible. In fact, in the thermodynamic limit, $N \to \infty$, the time evolution of the densities described by (6) converge, over a finite time interval, to the solutions of the following system of differential equations

$$\begin{cases} \dot{x} = (1 - x - y)[r_1 + (1 - r_1)\Theta(x - T)] - x \\ \dot{y} = x - r_2 y \end{cases} \tag{9}$$

which describes the deterministic evolution of the density of active and refractory units. Although we cannot obtain the full analytical solution of (9), we can study the system's equilibria and their stability. Indeed, by varying the threshold T, the dynamics switches between two different regimes based on the value of $\Theta[\cdot]$, as we see in figure 1. These two phases are characterized by high and low levels of activity, respectively. We call them super- and sub-critical phases.

The super-critical phase is defined by the condition $x > T$, for which the Heaviside function in (9) evaluates to 1. Hence, and at stationarity, we find

$$\begin{cases} y_+ = \dfrac{1}{2r_2 + 1} \\ x_+ = r_2\ y_+ \end{cases} \tag{10}$$

so that in this regime the average activity x_+ is independent of the rate of self-activation r_1. This means that the spread of activity is completely driven by the interaction between active neighbors. For this equilibrium to exist, we need

$$T < \frac{r_2}{2r_2 + 1} =: T_+ \tag{11}$$

so that the inequality $x > T$ is satisfied. This defines the threshold below which the super-critical phase exists.

Likewise, the sub-critical phase is defined by $x \leqslant T$. At stationary, (9) leads to

$$\begin{cases} y_- = \dfrac{r_1}{r_2 + (r_2 + 1)r_1} \\ x_- = r_2\ y_- \end{cases}, \tag{12}$$

and the inequality $x \leqslant T$ implies that

$$T \geqslant \frac{r_1 r_2}{r_2 + (r_2 + 1)r_1} =: T_-, \tag{13}$$

i.e., above the threshold T_-, the sub-critical phase exists. As expected, from (10) and (12) we notice that $\forall\, r_1, r_2$ the fraction of active nodes x_+ in the supercritical phase is larger than the subcritical equilibrium x_-, since

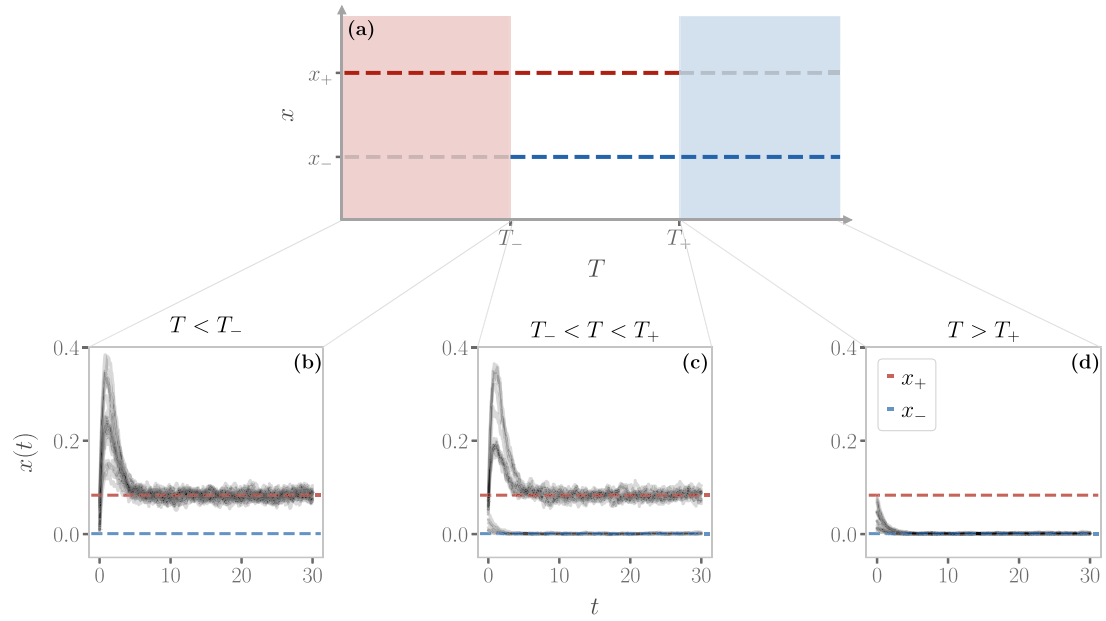

Figure 1. Diagram of equilibria in the model. (a) The region of existence of super- and sub-critical equilibria. As the control parameter T changes, we can identify three different regions: for low T, only the supercritical equilibrium exists (*red region*); for high T, only the subcritical equilibrium exists (*blue region*); for intermediate values of T, the two equilibria coexist. (b)–(d) Examples of trajectories in the three regions. Model simulated with a fully-connected network of size $N = 10^3$. Each plot shows 30 trajectories from a random initial configuration.

$r_1 \leqslant 1$. Moreover, in the range of T given by equations (11) and (13) for which such solutions exist, they are both stable equilibria, each with its own basin of attraction (see appendix B for an extensive analysis).

Crucially, and $\forall\, r_1, r_2$, (11) and (13) imply that $T_- < T_+$, thus three regions emerge in the parameter space spanned by T, as shown in figure 1. For $T \leqslant T_-$, the sub-critical equilibrium does not exist, hence we can only observe the super-critical equilibrium. On the other hand, for $T > T_+$ only the sub-critical equilibrium exists. In between these values, for $T_- < T \leqslant T_+$, the two equilibria coexist and we find a region of bistability.

3.2. Power spectrum

Neural activity typically exhibits a certain level of stochastic fluctuations, even when the brain is at rest. In fact, a growing amount of evidence suggests that neural noise might enhance the signal processing capabilities of neurons [39, 40]. To this end, we explore analytically the presence of oscillations in the model through the stochastic linearization obtained via a system size expansion [38], from which we derive the temporal evolution of the fluctuations around the equilibria (see appendix C). Indeed, this approach has been proven to be effective in other neuronal models [27, 41–43]. We find that the power spectrum in the super-critical regime is given by

$$S_x^+(\omega) = \frac{2r_2[1 + r_2 + r_2^2 + \omega^2]}{(1 + 2r_2)[(1 + 2r_2)^2 + (2 + r_2^2)\omega^2 + \omega^4]}, \tag{14}$$

and in the sub-critical regime we have

$$S_x^-(\omega) = \frac{2r_1r_2[r_1^2 + r_1r_2 + r_2^2 + \omega^2]}{(r_1 + r_2 + r_1r_2)[(r_1 + r_2 + r_1r_2)^2 + (1 + r_1^2 + r_2^2)\omega^2 + \omega^4]}. \tag{15}$$

Power spectra obtained from the simulation of the model are perfectly matched by these theoretical expressions, as we see in figure 2.

Equations (14) and (15) show that, in both regimes, for low frequencies the power spectrum is flat. On the other hand, in the large frequency limit, we find Brownian noise, i.e., $S(\omega) \approx \omega^{-2}$. Such scale-free behavior of the frequencies' spectrum is found, for instance, in local field potentials, i.e., the electrical activity of the brain measured with single microelectrodes [44].

Notably, in the super-critical regime, (15) does not display any peak. A small peak at

$$\omega_-^{\max} = [(1 + r_1r_2)(r_1r_2)^{1/2} - r_1^2 - r_2^2 - r_1r_2]^{1/2} \tag{16}$$

emerges instead in the sub-critical phase (15) for the range of parameters in which $\omega_-^{\max}$ exists, i.e., the radical is non negative. These results suggest that in the mean-field limit of the model, stochastic amplifications alone are not sufficient to induce significant sustained collective oscillations.

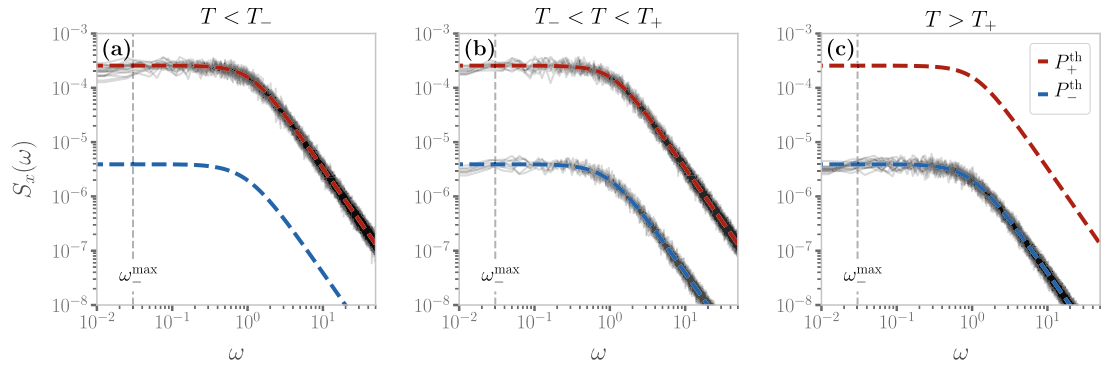

Figure 2. Theoretical expressions of the power spectrum are well-matched by simulated data from a fully-connected network at stationarity. The gray lines represent the power spectrum obtained by simulating the continuous-time model for 10^5 steps at stationarity in a network of $N = 10^3$ nodes and after an initial transient of 5×10^4 steps. (a) For $T < T_-$ the power spectrum shows a small peak at $\omega_-^{\max}$. (b) In the bistable region, depending on which equilibria the dynamics settles, we can find both power spectra. (c) For $T > T_+$, no peak emerges in the power spectrum.

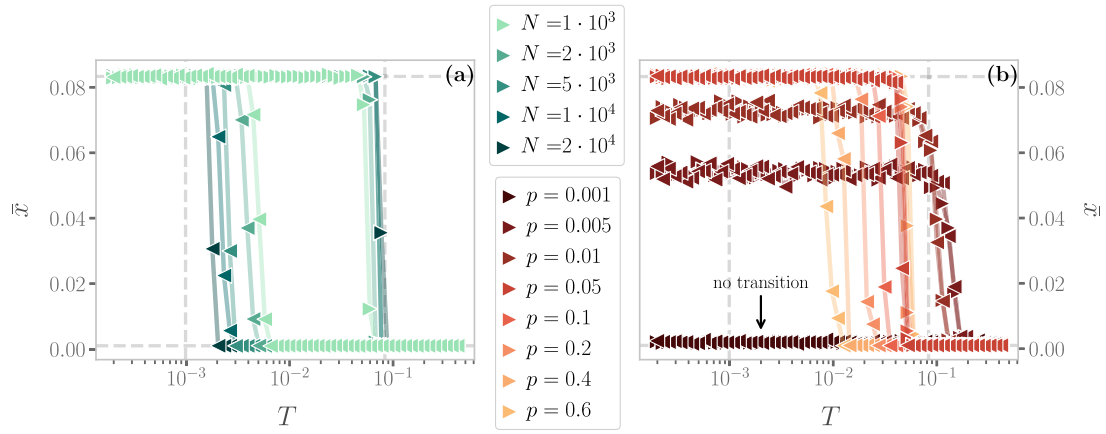

Figure 3. Average activity $\bar{x}$ as a function of the control parameter T for different sizes and topologies. To prove the presence of the bistable region, we slowly change T every 10^5 steps starting from $T_0 = 0.2 \cdot T_-$ up to $T_F = 5 \cdot T_+$ for 60 values of T taken in a logarithmic scale, and then decreasing it back to T_0 in the same way. (a) Results obtained with fully-connected topologies of different sizes N. Triangles to the right represent values obtained, while increasing T, whereas triangles to the left represent values obtained while decreasing it. We see that an hysteresis cycle emerges, and that it approaches the expected boundaries of the bistable region as N increases. (b) Results obtained from Erdős–Rényi networks with $N = 10^3$, constant weights and for different wiring probabilities p. As the connectivity decreases, the bistable region shrinks and the transition between the two regimes becomes smooth. For extremely low values of p, the transition disappears (as indicated by the arrow) and the system is never in the super-critical regime.

3.3. Finite-size effects

In order to assess the effects of finite sizes on the region of bistability, we track the average activity $\bar{x}$ as an order parameter following the approach used in [34]. The simulation starts at $T_0 = 0.2 \cdot T_-$ from a random initial configuration and, after a given number of steps, we increase the control parameter T by a small ΔT without resetting the state of the system. Such procedure is repeated up to a final value $T_F = 5 \cdot T_+$. Then, the same procedure is repeated starting from T_F and decreasing T down to T_0. By doing so, if ΔT is small enough, in the coexistence region we should find a hysteresis cycle as a consequence of bistability. Since we want to properly span both the super- and sub-critical regions, and because of the different order of magnitude of the two theoretical thresholds ($T_- \approx 10^{-3}$, $T_+ \approx 10^{-1}$), we choose to take 60 logarithmic steps.

In figure 3(a) we plot the behavior of $\bar{x}$ at different steps of this procedure for fully-connected topologies with different sizes. In the super- and sub-critical region, $\bar{x}$ is in accordance with the theoretical predictions (10) and (12). In between the theoretical values of $T_\pm$, we recover the discontinuous transition and the hysteresis cycle previously found in [34, 36]. Perhaps unsurprisingly, for small network sizes the limits of the hysteresis cycle do not precisely match the expected values of T_+ and T_- given in (11) and (13). In fact, due to the finite size of the system, the associated noise contribution causes the bistable region to shrink as the size of the network is reduced.

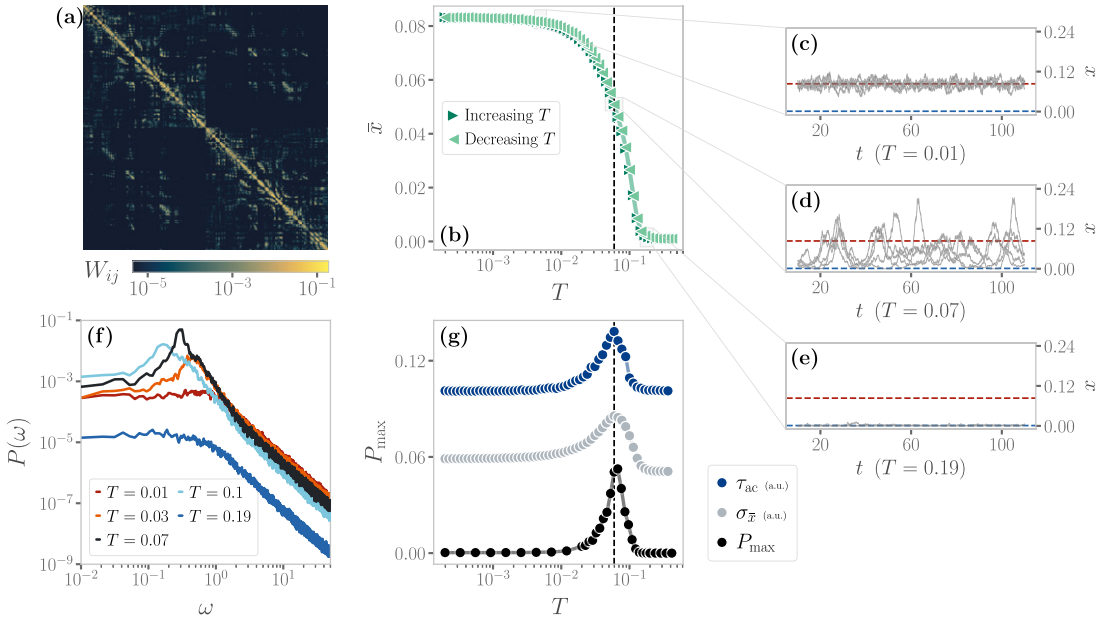

Figure 4. Dynamics of the model over an empirical connectome shows the emergence of a critical-like transition and collective oscillations. (a) Plot of the connectome from [32]. (b) The average activity $\bar{x}$ does not show any hysteresis cycle but rather changes smoothly from x_+ to x_- as T increases. (c)–(e) Examples of trajectories at different values of T. In particular, at intermediate values of T, the trajectories show high variability and a rich dynamics. (f) The power spectrum at different values of T. As $\bar{x}$ smoothly changes between the two equilibria, collective oscillations emerge. Notice that the frequency peak is at a frequency higher than $\omega_-^{\max}$. (g) The peak of the power-spectrum $P_{\max}$ is maximal at intermediate values of T. At the same point, both the autocorrelation time τ_{ac} and the variance $\sigma_{\bar{x}}$ of $\bar{x}$ peak (shown in arbitrary units), suggesting that a critical-like transition might be present.

3.4. Effects of the network structure

Insofar, we have considered the mean-field limit only, which corresponds to a fully-connected topology with constant weights. However, the architecture of the brain is usually characterized by sparse connectivity, and brain networks often display a non-trivial topology with small-world properties and community structures, both at the micro- and macro-scale. Moreover, the strength of the interaction between different brain regions is highly heterogeneous and typically follows a scale-free distribution [32, 45]. Hence, although eased by the homeostatic normalization [16], the hypothesis of constant weights is not fulfilled. In this section, we relax the first of these assumptions—a fully connected topology—at the price of analytical tractability.

We first study the simple case of an Erdős–Rényi network with a given wiring probability p between two nodes and constant weights [46]. We repeat the procedure described in section 3.3 at fixed network size, but for different wiring probabilities, see figure 3(b). We find that, as we lower the connectivity, the bistable region shrinks until it disappears, giving rise to a smooth transition at low values of p. This behavior, which is deeply different from the one expected from the mean-field approximation, is consistent with previous results obtained in the discrete time model [34, 37]. In the next section we show that such smooth transitions are strengthened by the introduction of empirical connectivity and they are crucial for the onset of emergent collective oscillations. Eventually, for very low values of p, the transition disappears as it becomes impossible for the network to sustain the super-critical regime.

3.5. Emergence of collective oscillations and continuous transitions

We now consider an empirical connectome of the human cerebral cortex with $N = 998$ regions [32]. In this case, we have both a complex topology and a non-trivial distribution of weights, as we see in figure 4(a). We find that, quite surprisingly, numerical simulations show that the analytical expressions of the two equilibria are still valid in the limit of small and large values of T. However, for intermediate values of the control parameter the average activity is no longer bounded to the two equilibria, but rather changes continuously from one to the other, as we see in figure 4(b).

In figures 4(c)–(e) we plot some trajectories for different values of T. We clearly see that, at intermediate values of T, the bistability is not present anymore—signaling that the transition is not first-order anymore, but rather happens in a continuous fashion. In particular, in figure 4(f) we show that the power spectrum now has a peak at these intermediate values—i.e., collective oscillations emerge. Crucially, the value of such peak $P_{\max}$ is maximal at intermediate values of T, where the average activity $\bar{x}$ is in between the equilibria $x_\pm$. In

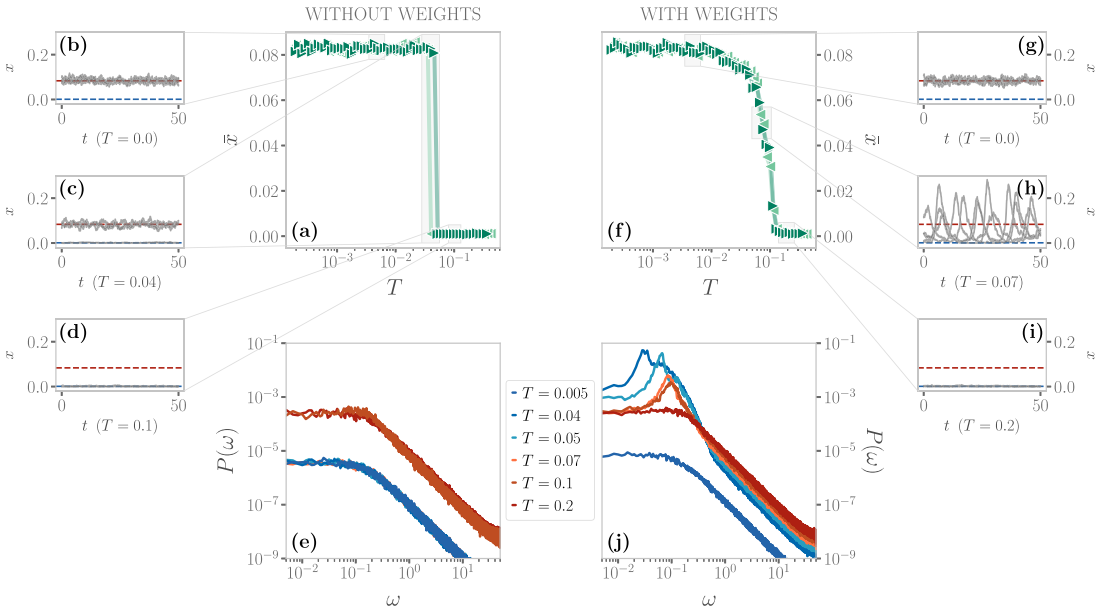

Figure 5. Dynamics of the model over an Erdős–Rényi network with wiring probability $p_{\text{conn}} \approx 0.08$, without and with weights following the empirical distribution of the connectome. (a)–(d) Without the weights, the transition is discontinuous with a bistable region, as we can see from both the hysteresis cycle and the trajectories. (e) No oscillations are present, and the power spectrum follows the mean-field prediction. (f)–(i) In the presence of the empirical weights, the transition becomes instead continuous. The trajectories in the region where the average activity $\bar{x}$ changes smoothly between $x_{\pm}$ display large departures from the expected equilibria. (j) With the empirical weights, oscillations are present.

figure 4(g) we show that at this particular value of T the variance of the activity $\sigma_{\bar{x}}$ peaks as well. Moreover, the activity shows long-range temporal correlations—indeed, the autocorrelation time τ_{ac}, computed as the characteristic decay time of the autocorrelation function, peaks at the same value of T.

These features are typically found in finite-size systems close to a second-order phase transition [47, 48], suggesting that they may emerge from a critical point of the control parameter T. Hence, the transition observed in the presence of the empirical connectome is reminiscent of criticality, rather than the bistability predicted by the mean-field limit. Let us stress that these features are emerging at the dynamical level, contrary to the percolation transition originally studied by Haimovici *et al* [18]. In general, we find that this dynamical transition does not occur at the same value of T of the percolation transition, as observed in other models [33].

In order to understand the relevance of the non-trivial topology of the connectome, we consider the Erdős–Rényi network previously studied, but with the same wiring probability of the connectome, $p_{\text{conn}} \approx 0.08$, and both with and without weights re-sampled from the empirical connectome weight distribution. As expected from figure 3, without the weights the wiring probability is high enough that the transition is discontinuous and a bistable region exists. In figures 5(a)–(e) we see that, in this scenario, the null model matches the behavior of the mean-field limit. No peak in the power spectrum emerges, and the stationary dynamics always reaches one of the two equilibria $x_{\pm}$.

These results change dramatically when we add back the weights from the empirical connectome. In figures 5(f)–(i) we see that no hysteresis cycle emerges, as the transition is now continuous and the system displays an oscillating behavior. Indeed, the power spectrum in figure 5(j) displays a clear peak, as we have previously shown for the connectome. That is, the presence of the empirical weights helps the disruption of the bistable region predicted at the mean-field level. Importantly, in appendix D we show that such a disruption emerges only if the wiring probability p of the Erdős–Rényi network is low enough. In fact, even with the empirical weights, the bistable region is still present in a fully connected network. This strongly suggests that a continuous, critical-like dynamical transition with global oscillations emerges if the underlying network is either extremely sparse—as in figure 3—or at higher values of p, but with a heterogeneous weight distribution. Crucially, empirical connectomes are often characterized by such features.

4. Discussion

Models of large-scale neuronal dynamics are fundamental in explaining and predicting neuronal activity at the macroscopic scale [30]. Such biophysically-inspired models, describing the collective behavior of populations of neurons, often replicate observed patterns of brain dynamics, e.g., scale-free avalanches [10, 15, 49],

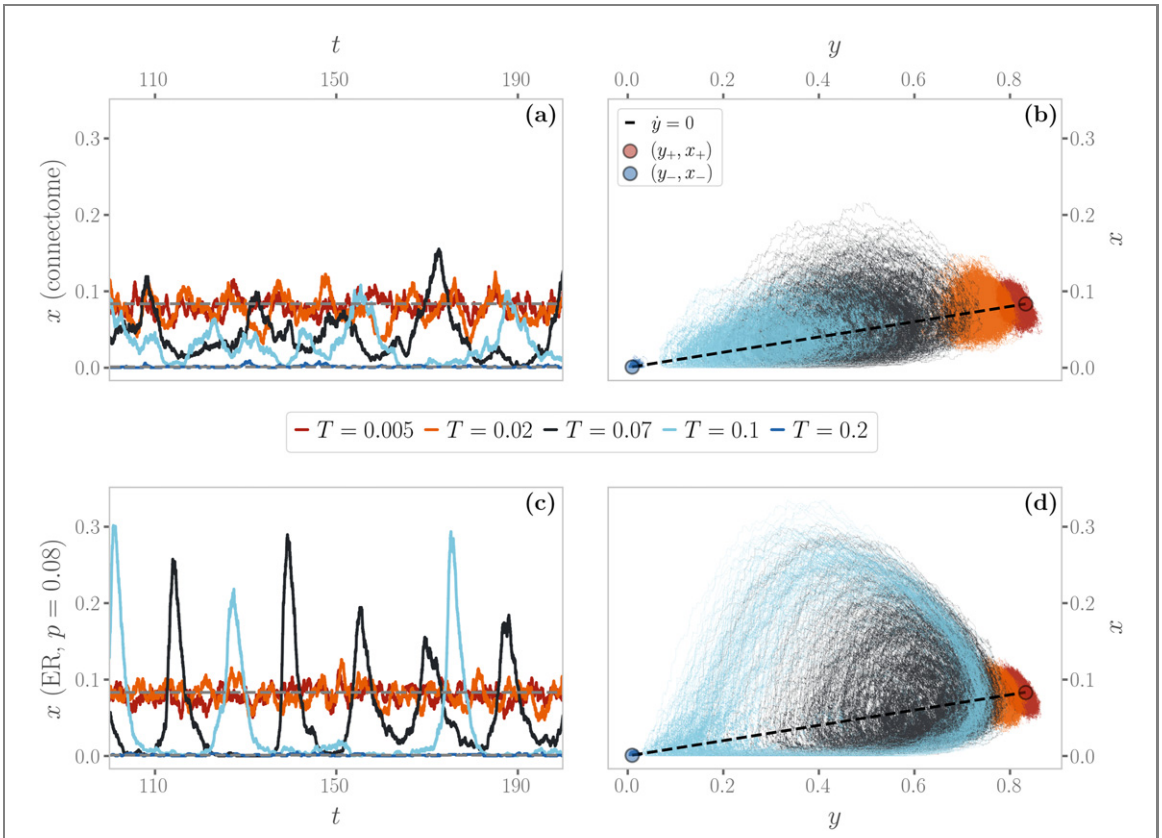

Figure 6. Comparison of the trajectories in the empirical connectome and in the Erdős–Rényi with $p = p_{\text{conn}}$ and empirical weights. (a) Connectome trajectories of x as a function of time and (b) in the phase space for different T. The black dashed line in panel (b) is the nullcline of the refractory population y, the gray lines in panel (a) are $x_{\pm}$. (c) and (d) Same, but in the case of the null model. Notice how the trajectories in the phase space are qualitatively different, and oscillations emerge as large activations from the sub-critical equilibrium (y_-, x_-).

long-range correlations [18, 19], global oscillations [25–27]. However, the collective dynamics is crucially determined both by the dynamical rules that model the inter-neuronal activations and by the geometry of their connections [34]. Furthermore, shared modulations of neural activity may play an important role and unexpectedly explain some of these properties [19, 50]. Disentangling these distinct contributions is a fundamental step toward gaining a deeper and more explicit understanding of the mechanisms behind the emergent patterns observed in the brain.

Driven by these considerations, in our work we have developed a continuous-time version of a whole-brain stochastic model [18] and we have studied the nature of the associated critical transition. Previous efforts often focused on the emerging percolation transition in the model, discussing the effect of the topology in shaping the transition by means of *in silico* [35, 36] and empirical connectomes [16, 37]. Here, we instead focus on the dynamical transition that arises in this model [34]. To the best of our knowledge, this study is the first attempt to investigate the nature and the consequences of this dynamical transition from an analytical perspective.

Yet, the bistable region found in the mean-field limit lacks any sign of collective oscillations. However, we have shown that this bistability can be disrupted by an interplay between the underlying network sparsity and a sufficiently heterogeneous weight distribution. Crucially, these properties are typically found in empirical connectomes of the human brain. In this scenario, the bistable region vanishes and a continuous critical-like transition emerges, with large autocorrelation times and variability of neural activity. At this transition, we also observe large collective oscillations, suggesting that both criticality and network structure play a fundamental role in driving the collective behavior of neurons.

Importantly, we can also compare the trajectories in the empirical connectome and in the null random network model with weights, see figure 6. In the empirical connectome, the dynamics is typically richer and oscillates close to the nullcline $\dot{y} = 0$ predicted by the mean-field (9). On the other hand, in the Erdős–Rényi case, the trajectories display large transient dynamics away from the (y_-, x_-) equilibrium, reminiscent of noise-induced oscillations [27, 41–43] or non-normal systems [51, 52]. This suggests that, although both models display emerging oscillations, the underlying dynamical features might be different. Notably, these phenomena have usually been observed in models with excitatory and inhibitory populations. Here, we rather have a

single excitatory population with a refractory state, hinting that the two different scenario may lead to a similar phenomenology. Therefore, further work is needed to explore the role of higher-order structures in the empirical connectome—e.g., modularity [53, 54] or heterogeneity [55] in the degree distribution—and their effect on the model dynamics.

The small size of the empirical connectome considered here may be a limitation for these investigations, since finite-size corrections may be hiding criticality. Notably, in [56] a similar modification of the discrete-time GH model run on a large-scale connectome displays semicritical behaviors consistent with a Griffith phase in a certain range of the control parameter. Such use of synthetic connectomes overcomes the finite size issue, at the cost of relying on some subjective assumptions about the generated topologies. Hence, future works should be devoted to fully understand whether the observed continuous transition is associated with a real critical point or with other phenomena such as rare region effects [57] or noise-induced transitions [43].

Overall, here we have shown in detail how network structure plays a fundamental, yet sometimes poorly understood, role. Therefore, we believe that our work will serve as a baseline for future analytical efforts in explaining the nature of the observed transition under more relaxed assumptions, e.g., in the presence of a non-trivial distribution of weights and different topologies, to further understand the influence of both in the emergence of critical features in the human brain. Possible approaches may include the use of heterogeneous mean-field methods as done in the study of epidemic spreading [55] or annealed network approximations [58]. All in all, we believe that our findings are a further contribution to the still puzzling 'critical brain hypothesis'.

Acknowledgments

SS acknowledges DFA and UNIPD for SUWE BIRD2020 01 Grant, and INFN for LINCOLN grant. We acknowledge Dr Rodrigo Rocha for pointing us to relevant literature. SS designed the study. SS and MF supervised the research. GB and GN performed the analytical calculations, implemented the simulations and prepared the figures. GB, GN, BM, MF and SS interpreted the results and wrote the manuscript. All authors contributed to the article and approved the submitted version.

Data availability statement

Data sharing is not applicable to this article as no new data were created or analysed in this study.

Code availability

The code of HTC model is available at https://github.com/gbarzon/HTC_Mesoscopic_Brain.

Appendix A. System size expansion in the mean-field approximation

The master equation (5) can be reframed in terms of the density of active x and refractory y neurons. Since $\Delta x = 1/N$, $\Delta y = 1/N$, we can treat them as continuous variables in the limit of a large system, i.e., $N \to \infty$, thus $P(x, y)$ becomes differentiable. By taking the continuum limit of the master equation (5) and by expanding all terms, i.e., the Kramers–Moyal expansion [38], up to the second order, we obtain the so-called Fokker–Planck equation for the probability density $p(x, y)$,

$$\begin{aligned}\frac{\partial}{\partial t}p(x,y) = &-\frac{\partial}{\partial x}[A_1(x,y)p(x,y)] + \frac{1}{2N}\frac{\partial^2}{\partial x^2}[B_{11}(x,y)p(x,y)]+\\ &-\frac{\partial}{\partial y}[A_2(x,y)p(x,y)] + \frac{1}{2N}\frac{\partial^2}{\partial y^2}[B_{22}(x,y)p(x,y)]+\\ &+\frac{1}{2N}\frac{\partial^2}{\partial x\partial y}[(B_{12}(x,y)+B_{21}(x,y))p(x,y)],\end{aligned} \tag{A.1}$$

where the coefficients are

$$\begin{cases} A_1(x,y) = (1-x-y)[r_1 + (1-r_1)\Theta(x-T)] - x \\ A_2(x,y) = x - r_2 y \\ B_{11}(x,y) = (1-x-y)[r_1 + (1-r_1)\Theta(x-T)] + x \\ B_{22}(x,y) = r_2 y + x \\ B_{12}(x,y) = -x \\ B_{21}(x,y) = -x \end{cases} \tag{A.2}$$

and $P(x,y) = p(x,y)\Delta x \Delta y$. The Fokker–Planck equation is a deterministic differential equation that describes how the probability distribution of states $p(x,y)$ evolves over time. Physically, it describes the evolution of an ensemble of systems: if we simulate a huge number of populations of neurons, all with the same parameters, they will have a different evolution due to random fluctuations, but the fraction of systems that have a density of states in $[x, x+\mathrm{d}x;\ y, y+\mathrm{d}y]$ at time t will be given exactly by $p(x,y)\mathrm{d}x\,\mathrm{d}y$ (in the limit of an infinite ensemble). An equivalent description can be derived by following instead a single population of neurons. In this case, a change in population density $[\mathrm{d}x, \mathrm{d}y]$ under the effect of stochastic fluctuations ξ is given by the associated Langevin equation (6) [38].

Appendix B. Stability analysis of equilibria

We further investigate the nature of the equilibria through linear stability analysis techniques. Indeed (9) is a dynamical system of the type:

$$\dot{\boldsymbol{z}} = \boldsymbol{f}(\boldsymbol{z}) \tag{B.1}$$

with $\boldsymbol{z} = (x,y)$ a two-dimensional vector. The equilibria $\boldsymbol{z}^*$ of this system are those that satisfy $\boldsymbol{f}(\boldsymbol{z}^*) = 0$. If we focus on the dynamics near the fixed points, we can make a change of variables $x = x^* + \Delta x$, $y = y^* + \Delta y$. In the limit of small variations $|\Delta \boldsymbol{z}| \to 0$, meaning that we are considering states infinitesimally near the fixed points, (B.1) can be Taylor expanded as

$$\begin{aligned} \Delta\dot{\boldsymbol{z}} &= \boldsymbol{f}(\boldsymbol{z}^*) + \left.\frac{\partial \boldsymbol{f}}{\partial \boldsymbol{z}}\right|_{z=z^*} \Delta \boldsymbol{z} + \cdots \\ &= \boldsymbol{J}(\boldsymbol{z}^*)\Delta \boldsymbol{z}. \end{aligned} \tag{B.2}$$

Thus the dynamics near the fixed points is governed, at the first order, only by the Jacobian matrix $\boldsymbol{J}$. In particular, the (real part of) the eigenvalues λ of $\boldsymbol{J}$ can give us information on stability or instability. If $\max \mathrm{Re}(\lambda) > 0$, the trajectories asymptotically diverge from the equilibria. Otherwise, for $\max \mathrm{Re}(\lambda) < 0$ the trajectories converge to the fixed point, which is stable in this case.

In the super-critical phase the Jacobian evaluated at (x_+, y_+) is

$$J_+ = \begin{bmatrix} -2 & -1 \\ 1 & -r_2 \end{bmatrix}. \tag{B.3}$$

The eigenvalues of (B.3) are

$$\lambda_+ = -\frac{2 + r_2 \pm \sqrt{r_2^2 - 4r_2}}{2}. \tag{B.4}$$

The stability condition holds if $\mathrm{Re}(\lambda_+) < 0$. We can distinguish two regimes: if $r_2 \geqslant 4$ the eigenvalues are purely real, otherwise they have an imaginary part. In both cases the conditions is satisfied, thus the super-critical fixed point (x_+, y_+) is respectively a *stable knot* and *stable focus* (figure B1).

Instead, in the sub-critical phase the Jacobian evaluated at $[x_-, y_-]$ is

$$J_- = \begin{bmatrix} -1 - r_1 & -r_1 \\ 1 & -r_2 \end{bmatrix} \tag{B.5}$$

whose eigenvalues are

$$\lambda_- = \frac{-(1 + r_1 + r_2) \pm \sqrt{(1 + r_1 + r_2)^2 - 4(r_1 + r_2 + r_1 r_2)}}{2}. \tag{B.6}$$

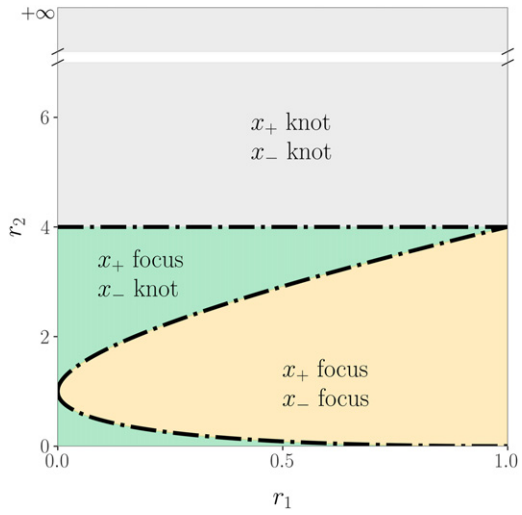

Figure B1. Type of fixed point in the parameter space (r_1, r_2).

The stability condition in this phase is again $\mathrm{Re}(\lambda_-) < 0$, which is satisfied $\forall\ r_1, r_2$ (since $r_1 \geqslant 0$ and $r_2 \geqslant 0$). We observe two different regimes by varying the parameters r_1 and r_2: if $r_1 - 2\sqrt{r_1} + 1 < r_2$ and $r_1 + 2\sqrt{r_1} + 1 > r_2$ the eigenvalues have an imaginary part, while in the other case they are pure real. So in the first cases the fixed point is a *stable focus*, while it is a *stable knot* in the other case (figure B1).

Appendix C. Power spectrum

To study the effect of fluctuations around the equilibrium we make use of the linear noise approximation [38]. First, we define here two local coordinates (ζ_1, ζ_2)

$$\begin{cases} x(t) = x^* + \dfrac{\zeta_x(t)}{\sqrt{N}} \\ y(t) = y^* + \dfrac{\zeta_y(t)}{\sqrt{N}} \end{cases} \Rightarrow \begin{cases} \zeta_x(t) = \sqrt{N}(x(t) - x^*) \\ \zeta_y(t) = \sqrt{N}(y(t) - y^*) \end{cases}. \tag{C.1}$$

In the Langevin equation, the stochastic fluctuations are of order $1/\sqrt{N}$, so here we multiply by $\sqrt{N}$ to remove this size dependence. Then, we rewrite the original equations in terms of (ζ_x, ζ_y), keeping only the linear terms. For the deterministic part, this leaves only the Jacobian evaluated at the equilibrium $J(x^*, y^*) \equiv J$. For the diffusion term we need to expand up to $1/\sqrt{N}$ (so then we get order 1 after multiplying by $\sqrt{N}$). But this means that b must be expanded to the 0th order, otherwise we would have terms in $1/N$, which become $1/\sqrt{N}$ after multiplication, which are negligible in the thermodynamic limit. After this we arrive at the following:

$$\begin{cases} \dot{\zeta}_x = J_{11}\zeta_x + J_{12}\zeta_y + \eta_x \\ \dot{\zeta}_y = J_{21}\zeta_x + J_{22}\zeta_y + \eta_y, \end{cases} \tag{C.2}$$

where

$$\begin{pmatrix} \eta_x \\ \eta_y \end{pmatrix} = \frac{1}{\sqrt{N}} \begin{pmatrix} C_1\xi_x + C_2\xi_y \\ D_1\xi_x + D_2\xi_y \end{pmatrix}. \tag{C.3}$$

Since ξ is Gaussian, also η is Gaussian. However, since in η we add different components of ξ, η_1 and η_2 are no longer uncorrelated:

$$\langle \eta_i(t) \rangle = 0 \qquad \langle \eta_i(t)\eta_j(t') \rangle = \delta(t - t')B_{ij}, \tag{C.4}$$

where $B_{ij} = B_{ij}(x^*, y^*)$ is the diffusion matrix evaluated at equilibrium. To proceed, we move to Fourier space. Since the transformation is linear, it preserves the linearity of the equations:

$$\begin{cases} \mathrm{i}\omega\tilde{\zeta}_x(\omega) = J_{11}\tilde{\zeta}_x + J_{12}\tilde{\zeta}_y + \tilde{\eta}_x \\ \mathrm{i}\omega\tilde{\zeta}_y(\omega) = J_{21}\tilde{\zeta}_x + J_{22}\tilde{\zeta}_y + \tilde{\eta}_y. \end{cases} \tag{C.5}$$

And the statistics of η remain the same:

$$\langle \tilde{\eta}_i(\omega) \rangle = 0 \qquad \langle \tilde{\eta}_i(\omega)\tilde{\eta}_j(\omega') \rangle = \delta(\omega - \omega')B_{ij}. \tag{C.6}$$

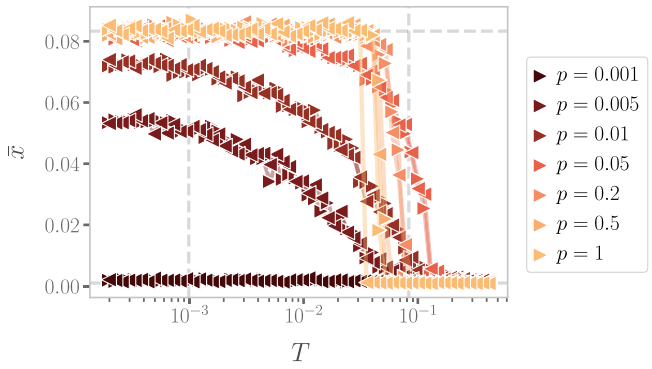

Figure D1. Average activity $\bar{x}$ in Erdős–Rényi networks at different wiring probabilities p, with weights re-sampled from the empirical connectome. With weights, the transition becomes continuous already at higher p.

The linear system (C.5) leads to:

$$\begin{cases} \tilde{\zeta}_x = \dfrac{(\mathrm{i}\omega - J_{22})\tilde{\eta}_x + J_{12}\tilde{\eta}_y}{-\omega^2 - \mathrm{i}\omega(J_{11} + J_{22}) + J_{11}J_{22} - J_{12}J_{21}} \\ \tilde{\zeta}_y = \dfrac{(\mathrm{i}\omega - J_{11})\,\eta_y \; + J_{21}\,\eta_x}{-\omega^2 - \mathrm{i}\omega(J_{11} + J_{22}) + J_{11}J_{22} - J_{12}J_{21}}. \end{cases} \tag{C.7}$$

Then we can study the power spectrum

$$S_i(\omega) = \langle \tilde{\zeta}_i(\omega)\tilde{\zeta}_i^*(\omega)\rangle = \langle \tilde{\zeta}_i(\omega)\tilde{\zeta}_i(-\omega)\rangle \tag{C.8}$$

that for the oscillations ζ_x of the density of active neurons x leads to

$$S_x(\omega) = \frac{\alpha + \beta\omega^2}{[(\omega^2 - \Omega_0^2)^2 + \Gamma^2\omega^2]}, \tag{C.9}$$

where

$$\begin{cases} \alpha = B_{11}J_{22}^2 - 2B_{12}J_{12}J_{22} + B_{22}J_{12}^2 \\ \beta = B_{11} \\ \Omega_0^2 = J_{11}J_{22} - J_{12}J_{21} \\ \Gamma^2 = (J_{11} + J_{22})^2. \end{cases} \tag{C.10}$$

Appendix D. Effects of empirical weights

Here, we show the effects of the addition of empirical weights to Erdős–Rényi networks. In figure 3 we have shown that with constant unitary weights and the homeostatic approximation, the bistability is still present at high wiring probabilities p. The transition only vanishes for very low p, and in this scenario the average activity in the super-critical regime is lower than the corresponding mean-field equilibrium x_+. In fact, if the wiring probability is too small, the network is too sparse to sustain activity. Notably, in this regime we find oscillations similar to the ones shown in figure 5(h), suggesting that the mechanism at play may be similar. However, the transition is still discontinuous at the wiring probability of the empirical connectome $p_{\mathrm{conn}} \approx 0.08$.

We now add weights re-sampled from the empirical connectome [32], and in figure D1 we show the average activity obtained while slowly varying T, as in the main text. First, let us note that in the fully-connected case $p = 1$, even with weights, a hysteresis cycle is still present. Hence, the transition is still discontinuous. However, the transition is now smoother already at higher values of p, showing that both sparsity and weights aid in the disruption of the bistability predicted by the mean-field approximation.

ORCID iDs

Giacomo Barzon https://orcid.org/0000-0002-9981-1027
Giorgio Nicoletti https://orcid.org/0000-0002-7682-0596
Benedetta Mariani https://orcid.org/0000-0001-7113-8806

Marco Formentin https://orcid.org/0000-0001-9865-5766
Samir Suweis https://orcid.org/0000-0002-1603-8375

References

[1] Leergaard T B, Hilgetag C C and Sporns O 2012 *Front. Neuroinf.* **6** 14
[2] Le Bihan D, Mangin J-F. o., Poupon C, Clark C A, Pappata S, Molko N and Chabriat H 2001 *J. Magn. Reson. Imaging* **13** 534–46
[3] Wedeen V J, Hagmann P, Tseng W-Y I, Reese T G and Weisskoff R M 2005 *Magn. Reson. Med.* **54** 1377–86
[4] Fox M D and Raichle M E 2007 *Nat. Rev. Neurosci.* **8** 700–11
[5] Beckmann C F, DeLuca M, Devlin J T and Smith S M 2005 *Phil. Trans. R. Soc.* B **360** 1001–13
[6] Damoiseaux J S, Rombouts S A R B, Barkhof F, Scheltens P, Stam C J, Smith S M and Beckmann C F 2006 *Proc. Natl. Acad. Sci. USA* **103** 13848–53
[7] Smith S M *et al* 2009 *Proc. Natl. Acad. Sci. USA* **106** 13040–5
[8] Spadone S, Della Penna S, Sestieri C, Betti V, Tosoni A, Perrucci M G, Romani G L and Corbetta M 2015 *Proc. Natl. Acad. Sci. USA* **112** 8112–7
[9] Priesemann V, Levina A and Wilting J 2019 Assessing criticality in experiments *The Functional Role of Critical Dynamics in Neural Systems* ed N Tomen, J Herrmann and U Ernst (Cham: Springer) pp 199–232
[10] Fontenele A J *et al* 2019 *Phys. Rev. Lett.* **122** 208101
[11] Levina A, Herrmann J M and Geisel T 2009 *Phys. Rev. Lett.* **102** 118110
[12] Wilting J and Priesemann V 2019 *Curr. Opin. Neurobiol.* **58** 105–11
[13] Hesse J and Gross T 2014 *Front. Syst. Neurosci.* **8** 166
[14] Buendía V, Di Santo S, Bonachela J A and Muñoz M A 2020 *Front. Phys.* **8** 333
[15] Beggs J M and Plenz D 2003 *J. Neurosci.* **23** 11167–77
[16] Rocha R P, Koçillari L, Suweis S, Corbetta M and Maritan A 2018 *Sci. Rep.* **8** 15682
[17] Korchinski D J, Orlandi J G, Son S W and Davidsen J 2021 *Phys. Rev.* X **11** 021059
[18] Haimovici A, Tagliazucchi E, Balenzuela P and Chialvo D R 2013 *Phys. Rev. Lett.* **110** 178101
[19] Mariani B, Nicoletti G, Bisio M, Maschietto M, Vassanelli S and Suweis S 2022 Disentangling the critical signatures of neural activity *Sci. Rep.* **12** 10770
[20] Meshulam L, Gauthier J L, Brody C D, Tank D W and Bialek W 2019 *Phys. Rev. Lett.* **123** 178103
[21] Nicoletti G, Suweis S and Maritan A 2020 *Phys. Rev. Res.* **2** 023144
[22] Markram H *et al* 2015 *Cell* **163** 456–92
[23] Di Santo S, Villegas P, Burioni R and Muñoz M A 2018 *Proc. Natl. Acad. Sci.* **115** E1356–65
[24] Buendía V, Villegas P, Burioni R and Munoz M A 2021 *Phys. Rev. Res.* **3** 023224
[25] Le Van Quyen M and Bragin A 2007 *Trends Neurosci.* **30** 365–73
[26] Begleiter H and Porjesz B 2006 *Int. J. Psychophysiol.* **60** 162–71
[27] Apicella I, Busiello D M, Scarpetta S and Suweis S 2021 *Neurocomputing* **461** 716–26
[28] Suárez L E, Markello R D, Betzel R F and Misic B 2020 *Trends Cogn. Sci.* **24** 302–15
[29] Damoiseaux J S and Greicius M D 2009 *Brain Struct. Funct.* **213** 525–33
[30] Breakspear M 2017 *Nat. Neurosci.* **20** 340–52
[31] Greenberg J M and Hastings S P 1978 *SIAM J. Appl. Math.* **34** 515–23
[32] Hagmann P, Cammoun L, Gigandet X, Meuli R, Honey C J, Wedeen V J and Sporns O 2008 *PLoS Biol.* **6** e159
[33] Martín P V, Domínguez-García V and Muñoz M A 2020 *New J. Phys.* **22** 083014
[34] Diaz M M S, Trejo E J A, Martin D A, Cannas S A, Grigera T S and Chialvo D R 2021 *Phys. Rev.* E **104** 064309
[35] Haimovici A, Balenzuela P and Tagliazucchi E 2016 *Brain Connectivity* **6** 759–71
[36] Zarepour M, Perotti J I, Billoni O V, Chialvo D R and Cannas S A 2019 *Phys. Rev.* E **100** 052138
[37] Rocha R P, Koçillari L, Suweis S, De Grazia M D F, de Schotten M T, Zorzi M and Corbetta M 2020 *bioRxiv Preprint* 10.1101/2020.12.17.423349 (retrieved 20 December 2020)
[38] Gardiner C W *et al* 1985 *Handbook of Stochastic Methods* vol 3 (Berlin: Springer)
[39] McDonnell M D and Ward L M 2011 *Nat. Rev. Neurosci.* **12** 415–25
[40] Guo D, Perc M, Liu T and Yao D 2018 *Europhys. Lett.* **124** 50001
[41] Bressloff P C 2010 *SIAM J. Appl. Math.* **70** 1488–521
[42] Fanelli D, Ginelli F, Livi R, Zagli N and Zankoc C 2017 *Phys. Rev.* E **96** 062313
[43] Wallace E, Benayoun M, van Drongelen W and Cowan J D 2011 *PLoS One* **6** 1–16
[44] Milstein J, Mormann F, Fried I and Koch C 2009 *PloS One* **4** e4338
[45] Bullmore E and Sporns O 2009 *Nat. Rev. Neurosci.* **10** 186–98
[46] Erdös P and Rényi A 2011 On the evolution of random graphs *The Structure and Dynamics of Networks* vol 6 (Princeton: Princeton University Press) pp 38–82
[47] Ma S k 2018 *Modern Theory of Critical Phenomena* (Routledge)
[48] Marro J and Dickman R 1999 *Nonequilibrium Phase Transitions in Lattice Models* (Cambridge: Cambridge University Press)
[49] Mariani B, Nicoletti G, Bisio M, Maschietto M, Oboe R, Leparulo A, Suweis S and Vassanelli S 2021 *Front. Syst. Neurosci.* **15** 709677
[50] Nicoletti G and Busiello D M 2021 *Phys. Rev. Lett.* **127** 228301
[51] Benayoun M, Cowan J D, van Drongelen W and Wallace E 2010 *PLoS Comput. Biol.* **6** e1000846
[52] Di Santo S, Villegas P, Burioni R and Muñoz M A 2018 *J. Stat. Mech.* 073402
[53] Villegas P, Moretti P and Muñoz M A 2015 *Sci. Rep.* **4** 1–7
[54] Ódor G and Kelling J 2019 *Sci. Rep.* **9** 1–10
[55] Pastor-Satorras R and Vespignani A 2001 *Phys. Rev.* E **63** 066117
[56] Ódor G, Gastner M T, Kelling J and Deco G 2021 *J. Phys.: Complex.* **2** 045002
[57] Vojta T 2006 *J. Phys. A: Math. Gen.* **39** R143
[58] Dorogovtsev S N, Goltsev A V and Mendes J F F 2008 *Rev. Mod. Phys.* **80** 1275